HTML ABSTRACT + LINKS

Suppression of inelastic deformation of nanocoated thin film microstructures

Yanhang Zhang,[a] Martin L. Dunn, and Ken Gall
Department of Mechanical Engineering, University of Colorado at Boulder, Boulder, Colorado 80309

Jeffrey W. Elam
Department of Chemistry and Biochemistry, University of Colorado at Boulder, Boulder, Colorado 80309

Steven M. George
Department of Chemistry and Biochemistry and Department of Chemical Engineering, University of Colorado at Boulder, Boulder, Colorado 80309

(Received 22 December 2003; accepted 11 March 2004)

We study the suppression of time-dependent inelastic deformation due to creep, stress relaxation, and microstructural evolution in multilayer thin film microstructures by the use of alumina nanocoatings realized by atomic layer deposition (ALD). Gold (0.5 μm thick)/polysilicon (1.5 or 3.5 μm thick) beam and plate microstructures were fabricated using surface micromachining. The microstructures were then coated on each side with a 40-nm-thick amorphous Al_2O_3 layer by ALD. The beam and plate microstructures were initially thermal cycled between room temperature and 190 °C to partially stabilize the gold microstructure. After the initial thermal cycles, the microstructures were cooled from 190 to 120 °C and held at 120 °C for about 700 h (4 weeks). We measured, using an interferometric microscope with a custom-built temperature chamber, full-field deformed shapes (and from these determined the average curvatures in the x and y directions) of the microstructures during the initial thermal cycles, during the cooling process from 190 to 120 °C, and during the isothermal hold. Measurements were made on both coated and uncoated microstructures to assess the influence of the coating. We find that while the 40-nm-thick coating has a small effect on the thermoelastic response of the microstructure, it significantly reduces the extent of inelastic deformation during the isothermal hold. We modeled the curvature evolution with time assuming the inelastic deformation mechanism can be described by power-law creep in the gold, $\dot{\epsilon}=A\sigma^n$, and that the polysilicon and alumina deform elastically. The simple model describes the observed behavior reasonably well for the uncoated microstructures (when the power-law parameters are fit using the measured curvature), however, for the coated microstructures, the model predicts a decrease in the inelastic deformation, but nowhere near the magnitude observed. This suggests not only an alternation of the stress state in the gold film by the nanoscale coating, but also a change in the fundamental inelastic deformation mechanisms. © *2004 American Institute of Physics.*
[DOI: 10.1063/1.1736329]

I. INTRODUCTION

Multilayer thin film material systems play a prominent role in numerous applications in microelectronics, optoelectronics, magnetic recording, and microelectromechanical systems (MEMS). An inherent characteristic of such systems is that misfit strains in the film layers lead to stresses in the layers and deformation of the structure upon temperature changes and during isothermal holds. For many applications, it is important to accurately control the deformation of thin film microstructures over a significant period of time in order to meet performance and reliability requirements. This is especially important for microstructures subjected to thermal loading and/or operated at elevated temperatures. When one or more of the layers consists of a metal or polymer film, inelastic deformation, due to the combined effects of creep and stress relaxation in the film, or microstructural evolution, can significantly influence deformation and compromise device performance. Our work is motivated by applications in MEMS where both short- and long-term dimensional stability are emerging as important issues for yield, performance, and reliability. For example, Miller *et al.*[1] fabricated microrelay switch arrays for RF communications applications using prestressed gold/polysilicon bimaterial beams as electrostatically actuatable switches. They observed a change in the switch shape and position over time and attributed it to stress relaxation in the gold. Vickers-Kirby *et al.*[2] report that creep in gold and nickel cantilever beams leads to voltage drops in micromachined tunneling accelerometers. These devices operate by applying a voltage to fix the position of the metal cantilever via electrostatic forces; a decrease in the voltage required means that less force is required to hold the cantilever in place. As will become apparent, inelasticity is especially interesting with MEMS-scale multilayer structures because the thin film layers are of comparable thicknesses. In

[a]Electronic mail: yanhang.zhang@colorado.edu

 © 2004 American Institute of Physics

Downloaded 12 Jul 2004 to 128.138.222.15. Redistribution subject to AIP license or copyright, see http://jap.aip.org/jap/copyright.jsp

this case the material nonlinearity can interact with geometric nonlinearity, significantly complicating the resulting deformation behavior.

Creep and stress relaxation phenomena have been investigated in some depth for thin film on thick substrate systems, motivated primarily by microelectronics applications.[3–7] Perhaps most closely connected to our work is the study by Shen and Suresh[5] of the effect of a thin passivation layer on stress relaxation response of metal films on thick silicon substrates. They found that when a SiO_2 passivation layer covered the aluminum film, the predicted stress relaxation based on power-law creep in the aluminum far exceeded that observed experimentally. They suggested that this means the SiO_2 passivation alters the deformation properties of the aluminum film. Thouless *et al.*[8] also studied the effect of a surface layer on the stress relaxation of thin films with a focus on the deformation mechanisms. Their experimental results suggest that the presence of a passivation layer on the surface of a film can have a substantial effect on relaxation rates, likely by suppressing mechanisms associated with diffusion and dislocation climb. Shen and Ramamurty[9] studied the thermomechanical behavior of passivated thin copper films and found that they do not exhibit significant stress relaxation at elevated temperatures. They attribute this to prevention of atomic diffusion along the surface and constrained dislocation motion due to the passivation. We have recently studied inelasticity at elevated temperatures and its effect on dimensional stability for a class of gold/polysilicon beam and plate microstructures for MEMS applications.[10] In the present work, we show that thin nanocoatings deposited using atomic layer deposition (ALD) can greatly reduce time-dependent inelastic deformation in thin film microstructures.

II. SAMPLES AND MEASUREMENTS

A. Test structures and fabrication process

We designed a series of gold/polysilicon beam and square plate microstructures and fabricated them using the MUMPs surface micromachining process, specifically MUMPs 42.[11] The process consists of the deposition and etching of a sequence of structural and sacrificial films. After all such processes, the microstructures are released by an etch in a 49% hydrofluoric acid solution for 4.5 min which removes the SiO_2 sacrificial material, rendering the microstructures free-standing. The thin film microstructures are then dried using a supercritical CO_2 drying process to prevent the beams from sticking to the substrate. The gold/polysilicon beam and plate microstructures consist of a 0.5 μm gold film on a 1.5-μm-thick (formed from the MUMPs Poly2 layer) or 3.5-μm-thick (formed from the MUMPs Poly1 and Poly2 layers) polysilicon film. We fabricated square ($L\times L$) plate microstructures of sizes $L=200$ and 300 μm, and 280 μm$\times$50 μm beam-like microstructures. The idea behind the design of the microstructures was to yield gold/polysilicon bilayer microstructures that were supported as freely as possible. To this end, the beams were cantilevered from the 2 mm$\times$2 mm silicon substrate by a 16 μm$\times$46 μm polysilicon support, and the plates were attached to the substrate by a 16-μm-diam polysilicon support in the center. Scanning electron micrographs of beam and plate microstructures are shown in Fig. 1.

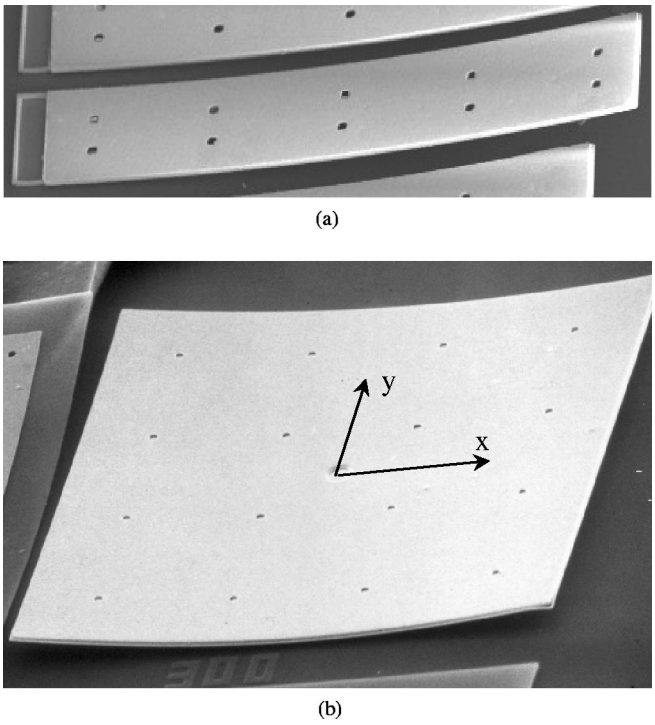

(a)

(b)

FIG. 1. Scanning electron micrograph of gold (0.5 μm thick)/polysilicon (1.5 μm thick) microstructures. The $x-y$ coordinate system used in subsequent measurements and analysis is identified: (a) 280 μm$\times$50 μm cantilever beam; (b) 300 μm$\times$300 μm square plate.

B. ALD nanocoating process

Atomic layer deposition (ALD) is a thin film growth technique that allows atomic-scale control of the growth process.[12,13] ALD utilizes a binary sequence of self-limiting chemical reactions between gas phase precursor molecules and a solid surface. The ALD process is illustrated in Fig. 2. The notches in the starting substrate for reaction (a) represent discrete reactive surface sites. Exposing this surface to reactant *A* results in the self-terminating adsorption of a monolayer of species *A*. The resulting surface then becomes the starting substrate for reaction (b). Subsequent exposure to molecule *B* will cover the surface with a monolayer of species *B*. Consequently, one (ab) cycle deposits one monolayer of the compound material *AB* and regenerates the initial substrate.

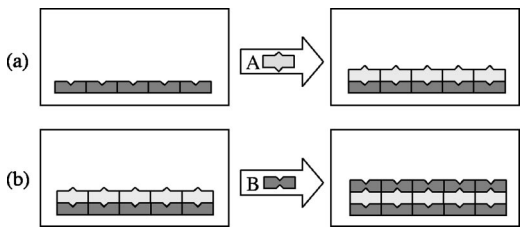

FIG. 2. Schematic illustration of binary reaction sequence for ALD.

Downloaded 12 Jul 2004 to 128.138.222.15. Redistribution subject to AIP license or copyright, see http://jap.aip.org/jap/copyright.jsp

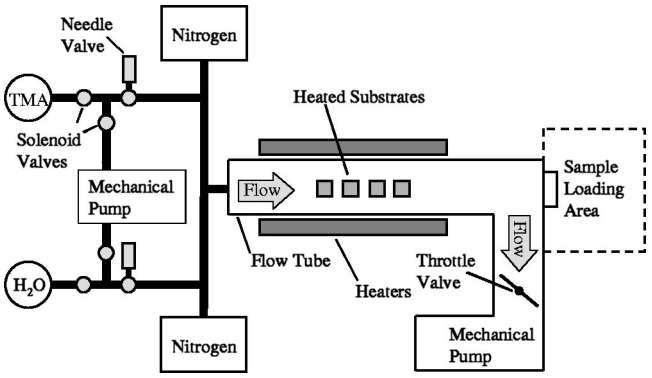

FIG. 3. Diagram of viscous flow reactor for atomic layer deposition.

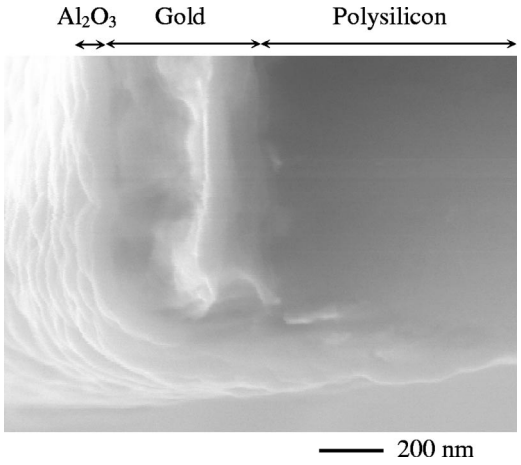

FIG. 4. Cross-sectional SEM image showing the conformal ALD Al_2O_3 coating on the corner of a gold/polysilicon beam. The beam was fractured by a micromanipulator prior to imaging.

By repeating the binary reaction sequence in an (abab...) fashion, a film of material can be deposited and the thickness of the ALD film can be controlled at the subnanometer level. Furthermore, because all of the surface sites are reacted during each (ab) cycle as illustrated in Fig. 2, the resulting ALD films are smooth, dense, and pinhole free. By allowing the gaseous reactant molecules to diffuse into voids and shadowed regions of the sample substrate, the ALD process enables substrates with complex geometries such as MEMS to be coated uniformly. This superb conformality has enabled the successful coating of powders, nanoporous membranes, and high aspect ratio trench structures. Atomic layer deposition techniques exist for depositing a variety of materials including oxides, nitrides, and metals.

The MEMS devices in this study were coated by ALD Al_2O_3 using alternating trimethyl aluminum (TMA) and H_2O exposures.[14] The A and B surface reactions that define an (ab) cycle for Al_2O_3 ALD are

$$\text{(a)}\quad \mathrm{AlOH}^* + \mathrm{Al(CH_3)_3} \rightarrow \mathrm{AlOAl(CH_3)_2^*} + \mathrm{CH_4},$$

$$\text{(b)}\quad \mathrm{AlCH_3^*} + \mathrm{H_2O} \rightarrow \mathrm{AlOH}^* + \mathrm{CH_4},$$

where the asterisks designate the surface species. The Al_2O_3 ALD was performed in a viscous flow ALD reactor[15] shown schematically in Fig. 3. The reactor is constructed using stainless steel components with all-metal seals. The MEMS substrates are held in the middle of a flow tube with a length of 60 cm and inside diameter of 3.5 cm. By resistively heating the outside of the flow tube, the MEMS substrates are maintained at 177 °C. Ultrahigh purity nitrogen gas at a mass flow rate of 200 sccm transports the reactive precursors to the samples and flushes the excess precursors and reaction products into a mechanical pump. A throttle valve located above the mechanical pump maintains a pressure in the flow tube of ~1 Torr.

Akzo Nobel semiconductor grade (99.9999%) TMA and Fisher Optima purity de-ionized H_2O reactant vapors are alternately pulsed into the nitrogen carrier gas stream to accomplish Al_2O_3 ALD. The gas switching for each reactant channel is performed using two computer-controlled solenoid valves and a needle valve.[15] This design enables a rapid switching between the TMA and H_2O precursors while allowing independent control of the pulse time and pressure. The needle valves for each reactant channel were adjusted to deliver pressure transients in the flow tube of $\Delta P \sim 0.1$ Torr. A nitrogen purge period is used after each reactant exposure to prevent mixing of the TMA and H_2O vapors.

The feasibility of applying Al_2O_3 ALD dielectric coatings to protect and electrically insulate MEMS cantilever test structures has been demonstrated recently.[16] Figure 4 shows a cross-sectional scanning electron microscopy (SEM) image of a gold (0.5 μm thick)/polysilicon (1.5 μm thick) beam coated with Al_2O_3. The Al_2O_3 coating layer is about 40 nm. In the present study, MEMS devices were coated using 310 ALD cycles for Al_2O_3 deposition. The coating was performed using exposure times of 2 s and purge times of 5 s at a temperature of 177 °C. These experimental conditions yield a growth rate for ALD Al_2O_3 of 1.29 Å/cycle on flat Si(100) surfaces.[17] Therefore, this process should generate an Al_2O_3 ALD film with a thickness of 40 nm on the MEMS devices. Before the coating process, the 2 mm×2 mm MEMS chip is bonded to a 1 in. by 3 in. silicon wafer strip (that can be put in the flow tube) using silver conductive epoxy and cured at 130 °C for 8 min. The entire coating process takes about 97 min at 177 °C including the loading and unloading process. After the coating process, the silicon wafer strip with the MEMS chip is heated to 140 °C for 5 min so the MEMS chip can be removed from the silicon wafer strip and put into the temperature chamber for subsequent measurements. In order to separate the effects of the Al_2O_3 coating and the thermal excursions experienced during deposition, we fabricated three series of samples with varying temperature histories as described in Table I.

TABLE I. Summary of the microstructures fabricated and the thermal history they were subjected to before testing.

Series	Al_2O_3 coating	Thermal history
1	40 nm thick	As-described for ALD
2	None	As-described for ALD
3	None	No temperature changes after release

Downloaded 12 Jul 2004 to 128.138.222.15. Redistribution subject to AIP license or copyright, see http://jap.aip.org/jap/copyright.jsp

C. Measurement procedures

We measured the deformation of the microstructures as a function of temperature change and holding time using an interferometric microscope and a custom-built thermal chamber that is covered by a quartz window to allow optical access. Full-field measurements of the out-of-plane displacement of the microstructures were made with scanning white light interferometry. The resolution of the out-of-plane displacement measurements, $w(x,y)$, is on the order of a nanometer as verified by making measurements on standard reference samples; the resolution of the temperature chamber is about 1 °C. During tests a 5× Michelson objective was used yielding a lateral spatial resolution of about 2.7 μm. Complete details regarding the testing procedures can be found elsewhere.[10,18] Our specific test protocol consists of the following:

(1) The microstructures are thermal cycled three times between room temperature and 190 °C to partially stabilize the gold microstructure.[10] The temperature is held constant for ≈3.5 min roughly every 15 °C so that thermal equilibrium is reached and measurements are made.
(2) After the initial thermal cycles, the microstructures are cooled from 190 to 120 °C, and then held at 120 °C for about four weeaks.
(3) Full-field displacements $w(x,y)$ are measured as a function of temperature during the initial thermal cycles, the subsequent temperature drop from 190 to 120 °C, and as a function of time during the isothermal hold at 120 °C.
(4) From the measured $w(x,y)$, we calculate the average curvatures $\kappa_x(x,y) \approx -\partial^2 w/\partial x^2$ and $\kappa_y(x,y) \approx -\partial^2 w/\partial y^2$ over a region of about 150 μm. For the plate microstructures the region is approximately 150 μm diameter around the center of each plate, while for the beam microstructures the region is of 150 μm length adjacent to the cantilever support. We measure only over this region, and not over the entire plate, because the slope of the displacement field outside this region is too large to be measured with the 5× objective. The average curvatures are then determined by fitting $w(x,y)$ with a second-order polynomial along $x=0$ and $y=0$, and then differentiating as appropriate.

III. OBSERVATIONS: BASIC PHENOMENA

Figure 5 shows the measured curvature versus temperature during the first three thermal cycles between 190 °C and room temperature for the three series of gold (0.5 μm thick)/polysilicon (3.5 μm thick) beam microstructures ($L = 280\ \mu$m). Although not shown, the plate and beam microstructures from the same series exhibit similar behavior, except that the magnitude of the curvature differs accordingly.

Figure 5(a) shows the curvature for the *series 3* microstructures, i.e., the as-released microstructures. During the initial heating, the beam deforms linearly, until the temperature reaches about 80 °C. As the temperature is increased further to 190 °C, nonlinear behavior initiates and progresses. These phenomena have been observed in many metal films for microelectronics applications and we have studied it extensively for gold/polysilicon MEMS microstructures.[19] The

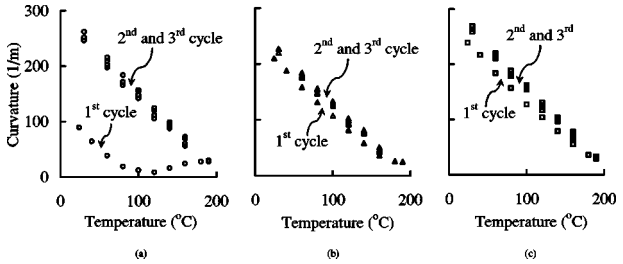

FIG. 5. Curvature measurements during thermal cycling between 190 °C and room temperature before the isothermal tests for gold (0.5 μm thick)/polysilicon (3.5 μm thick) 280 μm×50 μm beam microstructures. (a) *series 3*; (b) *series 1*; and (c) *series 2* microstructures.

nonlinear behavior likely results because the material microstructure of the evaporated film is not stable as deposited and the temperature increase during the first cycle promotes material microstructural changes in the film, such as annihilation of excess vacancies, void coalescence, and grain growth, that result in the development of tensile stresses in the gold film.[5,20–23] As the microstructure is cooled back to room temperature, the response is linear thermoelastic. Subsequent thermal cycles follow the same thermoelastic path suggesting that the gold material microstructure has partially stabilized, at least over this temperature–time cycle regime. More detail, including a simple model for the development of curvature during the first thermal cycle, is given by Zhang and Dunn.[19]

Figure 5(b) shows the curvature for the *series 1* microstructures, i.e., those coated with Al_2O_3 by ALD. As previously mentioned, before the thermal cycle measurements shown in Fig. 5, the coated beams have been subjected to thermal excursions during the ALD process, reaching a maximum temperature of 177 °C. As a result, coated beams are expected to deform linearly over a temperature range with a maximum temperature less than 177 °C (for a detailed discussion, please see Zhang and Dunn[19]). During the first cycle in Fig. 5(b), the coated beam deforms linearly when the temperature is increased from room temperature to about 180 °C. Further temperature increase to 190 °C results in nonlinear behavior. Upon cooling from 190 °C to room temperature, the curvature varies linearly with the temperature change. The second and third thermal cycles then appear to exhibit linear behavior with good repeatability from cycle to cycle. We note that large numbers of cycles (~1000) leads to ratcheting of the linear response and inelasticity in the gold.[24]

Figure 5(c) shows the curvature versus temperature for the *series 2* microstructures, i.e., those that were not coated, but subjected to the same temperature profile as the coated beams. Similar behavior is observed for Figs. 5(b) and 5(c), which seems to substantiate the claim that the maximum temperature reached controls the subsequent thermomechanical response. Although qualitatively similar, due to the thermoelastic stiffening caused by the Al_2O_3 coating, the *series 1* beams [Fig. 5(b)] exhibit a slightly lower curvature before and after the thermal cycles than the *series 2* beams [Fig. 5(c)].

Downloaded 12 Jul 2004 to 128.138.222.15. Redistribution subject to AIP license or copyright, see http://jap.aip.org/jap/copyright.jsp

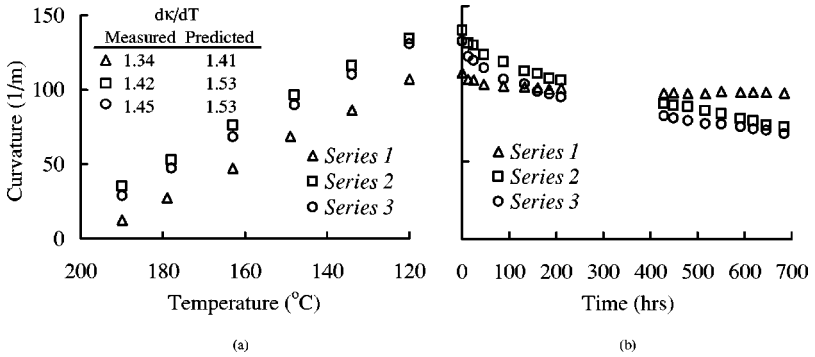

FIG. 6. (a) Measured curvature vs temperature during cooling from 190 to 120 °C (the thermoelastic slope is shown both from measurements and calculations); and (b) measured curvature vs time during the isothermal hold at $T=120\,^{\circ}\mathrm{C}$ for gold (0.5 μm thick)/polysilicon (3.5 μm thick) 280 μm×50 μm beam microstructures.

Figure 6(a) shows the curvature versus the temperature during cooling (after the initial thermal cycles) from 190 to 120 °C for 280×50 μm gold (0.5 μm thick)/polysilicon (3.5 μm thick) microbeams. Here and throughout the paper open squares represent the *series 2* microstructures; open circles represent the *series 3* microstructures; and open triangles represent the *series 1* microstructures. All of the beams show a linear thermoelastic response. The thermoelastic slope $d\kappa/dT$ from both the experiments and companion calculations are shown in Fig. 6(a).

The uncoated beams (*series 2 and 3*) have similar thermoelastic slopes; we suspect the small variation in curvature variation between the two series of uncoated beams is due to the differences from chip to chip. This is consistent with the observation of linear thermoelastic behavior in that the different temperature profiles experienced by the beams do not affect the thermoelastic response. Thus we can focus our attention on the effect of coating in the comparison between coated and all uncoated beams. Although not shown, this is also the case for the plate microstructures. The thermoelastic slope for the coated beams is about 10% less than that for the uncoated beams. This is because the Young's modulus of the Al_2O_3 coating layer is higher than the gold and polysilicon layer, so the effective stiffness of the coated beams is higher than the uncoated beams. Even though the coating is thin, the effect on the thermoelastic slope is measurable.

Figure 6(b) shows the curvature versus time during the isothermal hold at $T=120\,^{\circ}\mathrm{C}$ for the beam microstructures in Fig. 6(a). The starting point of Fig. 6(b) is the ending point of Fig. 6(a). During the isothermal hold, stress relaxation occurs in the gold film and results in tensile creep strain. The tensile straining of the film competes with the thermoelastic deformation, and this is manifested as a decrease in curvature of the microstructures. Over the hold period of 700 h, the curvature of the uncoated beams decreases by about 46% of the initial curvature. The two series of uncoated beams do not show significant differences, even though they were subjected to different initial temperature profiles. For the coated beams, the curvature decreases significantly only during the first 50 h, by about 7.5% of the initial curvature. During the reminder of the time, the curvature is essentially unchanged. Clearly, the Al_2O_3 coating substantially suppresses the inelastic deformation of the gold/polysilicon microbeam. This is consistent with studies regarding creep and stress relaxation in passivated metal films.[5,8,9]

IV. ANALYSIS

The thermoelastic deformation of multilayer beam microstructures can be predicted by the theory of linear thermoelasticity. This has been discussed in detail by Zhang and Dunn.[19] For beam microstructures with the coating, there is a Al_2O_3 layer both on the top and the bottom of the beam, therefore the beam has four layers: Al_2O_3 (40 nm thick), gold (0.5 μm thick), polysilicon (1.5 μm or 3.5 μm thick), and Al_2O_3 (40 nm thick). With an analysis similar to that by Zhang and Dunn,[19] the average curvature of a four-layer beam microstructure, κ, depends linearly on the thermal expansion mismatch strain and can be expressed as

$$k=\frac{A}{B}, \tag{1}$$

where

$$\begin{aligned} A=6T\Bigg(&\sum_{i=1}^{3} M_i M_{i+1} t_i t_{i+1}(t_i+t_{i+1})(\alpha_{i+1}-\alpha_i) \\ &+\sum_{i=1}^{2} M_i M_{i+2} t_i t_{i+2}(t_i+2t_{i+1}+t_{i+2})(\alpha_{i+2}-\alpha_i) \\ &+M_1 M_4 t_1 t_4(t_1+2(t_2+t_3)+t_4)(\alpha_4-\alpha_1)\Bigg), \end{aligned} \tag{2}$$

$$\begin{aligned} B=&\sum_{i=1}^{4} M_i^2 t_i^4+2\sum_{i=1}^{3} M_i M_{i+1} t_i t_{i+1}(2t_i^2+3t_i t_{i+1} \\ &+2t_{i+1}^2)+2\sum_{i=1}^{2} M_i M_{i+2} t_i t_{i+2}(2t_i^2+3t_i t_{i+2}+2t_{i+2}^2 \\ &+6t_{i+1}(t_i+t_{i+1}+t_{i+2}))+2M_1 M_4 t_1 t_4(2t_1^2+3t_1 t_4 \\ &+2t_4^2+6(t_2+t_3)(t_1+t_2+t_3+t_4)) \end{aligned}$$

In Eq. (1) we consider a four-layer beam with layer thickness t_1, t_2, t_3, and t_4. Each layer is assumed isotropic and characterized by Young's modulus E_i, Poisson's ratio v_i, thermal expansion coefficient α_i (i=1,2,3,4). $M_i=E_i/(1-v_i)$ is the biaxial modulus. T is the temperature change from a reference temperature where $\kappa=0$. For beam microstructures without the coating, only two layers exist: gold and polysilicon. The parameters for $i=3$ and 4 are set

Downloaded 12 Jul 2004 to 128.138.222.15. Redistribution subject to AIP license or copyright, see http://jap.aip.org/jap/copyright.jsp

to be zero in Eq. (1) and the average curvature for a two layer beam microstructure can be expressed in the well-known form:

$$k=\frac{6TM_1M_2t_1t_2(t_1+t_2)(\alpha_2-\alpha_1)}{M_1^2t_1^4+M_2^2t_2^4+2M_1M_2t_1t_2(2t_1^2+3t_1t_2+2t_2^2)}. \quad (3)$$

In Eqs. (1)–(3), we use the biaxial modulus instead of Young's modulus because for the fully covered beam microstructures discussed in this work, the curvature in the transverse direction differs insignificantly from that along the length of the beam. In other words, we must take account of the Poisson effect and treat these microstructures as plates.

The linear thermoelastic slope, $\eta=d\kappa/dT$, can be obtained from Eqs. (1) and (3) by straightforward differentiation for coated and uncoated beams, respectively. Furthermore, we use these analytical results primarily to assess the effect of the Al_2O_3 nanocoatings on the thermoelastic behavior or the microstructures. To model the inelastic thermomechanical deformation both during the temperature change and the constant temperature hold period, we use the ABAQUS finite element code. Specifically, we use composite shell elements to approximate the thin-plate kinematics of the Kirchhoff theory. All materials are modeled as linear elastic with isotropic material properties. Here and throughout the subscripts p, g, and a denote polysilicon, gold, and alumina, respectively. Input parameters to the finite element calculations are $E_p=163$ GPa, $\nu_p=0.22$ (in line with many measurements over many MUMPs runs[25]), $E_g=78$ GPa, $\nu_g=0.42$.[26] DelRio *et al.*[27] obtained $E_a/(1-\nu_a^2)=215$ GPa and we use $\nu_a=0.24$ in line with values reported by Proost and Spaepen to get $E_a=203$ GPa. The thermal expansion coefficients of polysilicon and gold were assumed to vary linearly with temperature, and values at 190(120) °C are $\alpha_p=3.5(3.2)\times10^{-6}/°C$, and $\alpha_g=15.1(14.6)\times10^{-6}/°C$.[26] The thermal expansion coefficient of alumina was assumed constant $\alpha_a=5.0\times10^{-6}/°C$.[28] Typical finite element meshes for the square plate microstructures contained square elements of dimension 12.5 μm×12.5 μm, a size that was chosen after a careful convergence study with mesh size.

The complete calculations consist of two parts. First, the thermomechanical deformation during the cooling process is computed. Details regarding these calculations are described elsewhere.[10] As will be seen, for larger plate microstructures the deformation response can consist of a bifurcation in the curvature from a spherical to an ellipsoidal deformation mode. The details of this bifurcation are extremely sensitive to imperfections and without a complete knowledge of these details it is difficult to accurately predict this. The second step of the calculations is the inelastic deformation during the isothermal hold. The starting point for these calculations is the ending point of the first calculation. In the case of the bifurcated plate, we tuned the results of the first calculation step to match the measured result by modifying the anisotropy in the thermal expansion mismatch. This effect is described by Dunn *et al.*,[18] and has no impact on the thermomechanical response prior to the bifurcation. We modeled inelastic deformation by assuming a simple power-law strain rate dependence of the gold, $\dot{\epsilon}=A\sigma^n$, and assuming the polysilicon and alumina only deformed elastically at the modest temperature of 120 °C. The material constants n and A are determined by fitting the calculations to the entire measurements for the beam microstructures.

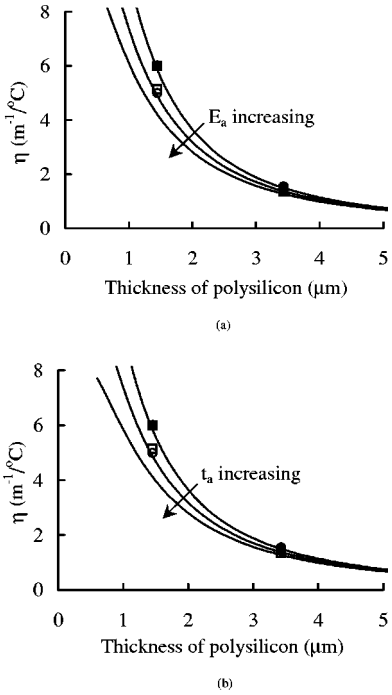

FIG. 7. Thermoelastic slope $\eta=d\kappa/dT$ vs polysilicon thickness for beam microstructures. (a) Effect of the Young's modulus of the Al_2O_3 coating layer. The thickness of the Al_2O_3 layer is $t_a=40$ nm. The curves from right to left are for the $E_a=0$, 203, and 400 GPa, respectively; and (b) effect of Al_2O_3 coating thickness on η. The Young's modulus of the Al_2O_3 layer is $E_a=203$ GPa. The curves from right to left are for $t_a=0$, 40, and 100 nm, respectively. Curves are analytical result from Eq. (1); circles are finite element calculations, and squares are measurements; open symbols are for the coated beam microstructures and closed symbols are for the uncoated beam microstructures.

V. RESULTS AND DISCUSSION

In Fig. 7 we plot the thermoelastic slope $\eta=d\kappa/dT$ versus polysilicon thickness for the microbeams, where the thickness of gold is fixed at 0.5 μm. In Fig. 7(a) we study the effect of Young's modulus of the Al_2O_3 coating layer. The measured thickness of the Al_2O_3 coating layer is $t_a=40$ nm. The various solid curves represent the analytical results for different values of Young's modulus of the alumina using Eqs. (1) and (3). The $E_a=0$ GPa curve corresponds to the uncoated beam microstructures. The closed symbols are finite element calculations (circles) and measurements (squares) for the uncoated beams. At the resolution of the plot the symbols overlap for the $t_p=3.5$ μm microbeams. The analytical result, finite element calculations, and measurements agree well for the uncoated beam microstructures. For the coated beam microstructures, the thermoelastic slope $d\kappa/dT$ will be slightly decreased due to the stiffening from the Al_2O_3 coating layer, as we can see by the comparison between the measurements for coated (open squares) and uncoated (closed squares) beam microstructures. For thicker polysilicon (e.g., $t_p=3.5$ μm), the effect of

Downloaded 12 Jul 2004 to 128.138.222.15. Redistribution subject to AIP license or copyright, see http://jap.aip.org/jap/copyright.jsp

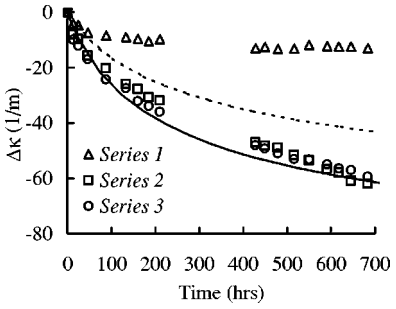

FIG. 8. Measured and predicted curvature change during the isothermal hold at 120 °C of 280 μm×50 μm gold (0.5 μm thick)/polysilicon (3.5 μm thick) beam microstructures. Open symbols represent the measurements and curves are calculations without (solid line) and with (dashed line) the coating.

the coating layer on the thermoelastic slope becomes insignificant at the scale of the plot. The Young's modulus of bulk Al_2O_3 is about 400 GPa.[29] However, we can see from Fig. 7(a) that with $E_a = 400\,\mathrm{GPa}$, the thermoelastic slope is significantly underestimated; this is clearly seen for $t_p = 1.5\,\mu\mathrm{m}$. The high modulus reported for bulk crystalline Al_2O_3 reflects the fact that it is crystalline, however the ALD nanocoatings are amorphous and thus would be expected to have a much lower Young's modulus as compared with the bulk material. Even though it is not our emphasis, from Fig. 7 we infer the Young's modulus from the measurement by comparing the thermoelastic slope between the calculations and measurements. From Fig. 7(a), we can see that with $E_a = 203\,\mathrm{GPa}$, we get better agreement between the calculations and measurement. Here we need to point out that our estimate of E_a is based on the unknown Poisson's ratio and thermal expansion coefficient of the ALD Al_2O_3 nanocoatings. Even though not shown here, calculations show that varying the thermal expansion coefficient of alumina from 5 to $20\times10^{-6}/°\mathrm{C}$ has an insignificant effect on $d\kappa/dT$. Our estimate does suggest that the Young's modulus of the amorphous Al_2O_3 nanocoatings is much lower than the bulk crystalline Al_2O_3.

In Fig. 7(b) we study the effect of Al_2O_3 coating thickness on $d\kappa/dT$ versus the polysilicon thickness with the Young's modulus of the Al_2O_3 layer fixed as $E_a = 150\,\mathrm{GPa}$. The curve for $t_a = 0\,\mu\mathrm{m}$ corresponds to the uncoated beam microstructures. As the thickness of the coating layer increases, the thermoelastic slope of the coated structure decreases. The significance of the stiffening effect of the coating layers on the thermoelastic slope increases as the thickness of the polysilicon decreases. Although not shown on the plot, in the limit as the polysilicon layer goes to zero, the structure becomes just a single gold layer with symmetric coatings on both the top and the bottom and therefore no curvature develops and $d\kappa/dT = 0$.

In Fig. 8 we plot the measured and predicted curvature change (from the curvature after cooling) versus time during the isothermal hold for each series of microbeams in Fig. 6. The difference between the experimental curvature changes in the coated and uncoated beams shows the substantial effect of the coating layer on inelastic deformation. The two series of the uncoated microstructures, *series 2* and *series 3*, show no significant difference. Recall that the only difference between them is that the microstructures of *series 2* have the same thermal history as the ALD coated microstructures, i.e., *series 1*. This suggests that the thermal history during the coating process does not contribute to the response of the ALD coated microstructures, and thus the response is due to the coating itself. The solid line shows a calculation that was fit to the measurements for uncoated beams by assuming simple power-law inelastic deformation of the gold film. With $n = 5$ and $A = 9\times10^{-16}\,\mathrm{h}^{-1}\,\mathrm{MPa}^{-5}$, the deformation behavior over a time period of about 700 h (4 weeks) is well described. While these parameters were chosen to fit the data, they are in reasonable agreement with thin film data in the literature as described earlier, particularly, the power-law exponent. We have studied the effects of the power law constants A and n of the gold film[10] on the curvature evolution during the isothermal hold. The overall responses are qualitatively similar, making it difficult to separate the two without further information. We do not know the detailed mechanisms that are operative, and we can find no data in the literature in this stress–temperature regime. Furthermore, the deformation mechanism maps are typically altered for thin film versus bulk metals, especially at low stresses.

During the isothermal hold, inelastic deformation occurs in the gold film and this is manifested as a decrease in curvature of the microstructure. Over the hold period of 700 h, the curvature of the uncoated beams decreases by about 60 m^{-1}, which is about 43% of the initial curvature. However for the coated beam, the curvature decreases only about 12 m^{-1}, about 12% of the initial curvature. The dashed line shows calculations using the same power-law parameters, but with a 40-nm-thick elastic Al_2O_3 coating on each side of the beam. As expected, the calculation shows a decrease in the curvature change with temperature, but nowhere near the magnitude of that observed. This suggests that not only is the stress state in the gold film altered by the nanoscale coating, but also that the fundamental deformation mechanisms are altered. These likely include the suppression of diffusion along the surface of the film and prevention of dislocation motion. We tried to characterize the microstructure before and after the tests for coated and uncoated beams and plates using high resolution SEM (scanning electron microscopy), but this surface characterization revealed no significant differences. Microstructural characterization through the thickness is very challenging with these small samples. We are in the process of using field-emission scanning electron microscope and transmission electron microscopy to do this. Fortuitously, at least from the viewpoint of dimensional stability, is the fact that the coating dramatically reduces the inelasticity. The actual response of the coated microstructures cannot be modeled by the simple power law formulation, at least with the same parameters. This is consistent with results for aluminum films on thick silicon substrates covered by a SiO_2 passivation layer.[5,8,9]

In Fig. 9 we show corresponding results for $L = 200$ and 300 μm plate microstructures of the same thickness (0.5-μm-thick gold and 3.5-μm-thick polysilicon) as the beams in Fig. 8. We measured curvatures in both x and y directions

Downloaded 12 Jul 2004 to 128.138.222.15. Redistribution subject to AIP license or copyright, see http://jap.aip.org/jap/copyright.jsp

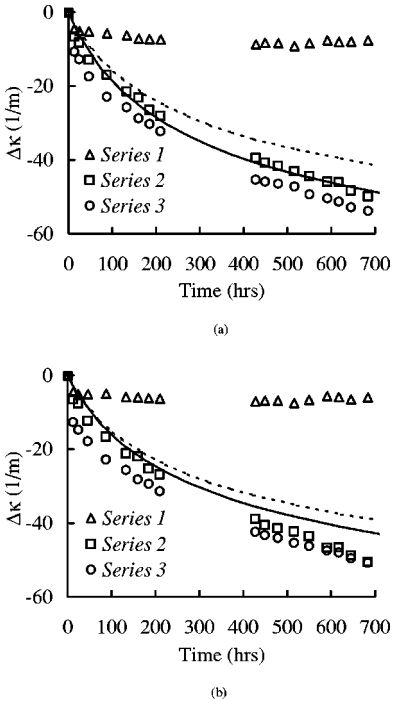

FIG. 9. Measured and predicted curvature change during the isothermal hold at 120 °C of (a) 200 μm×200 μm; and (b) 300 μm×300 μm gold (0.5 μm thick)/polysilicon (3.5 μm thick) plate microstructures. Open symbols represent the measurements and curves are calculations without (solid line) and with (dashed line) the coating.

and they are roughly the same so for ease of viewing in Fig. 9 we show only the curvature in x direction (The differences between κ_x and κ_y are insignificant at the scale of the plot, less than 2% of the averaged between κ_x and κ_y). The effect of the coating layer on the curvature of the plate microstructures is similar to that shown in Fig. 7 for the beams. Calculations done using the n and A determined from the fit to the data for beams in Fig. 8 agrees well with the measurements for the uncoated plates over the isothermal hold period. Again, for the coated plates, the calculation shows a decrease in the curvature change with temperature, but nowhere near the magnitude of that observed. In Figs. 9(a) and 9(b), there is a slight difference between the two series of uncoated microstructures, but it is not significant when compared to the difference between the coated and uncoated microstructures. The minor differences might result from chip to chip variations.

We also studied the isothermal deformation of microstructures with 0.5-μm-thick gold and 1.5-μm-thick polysilicon films. Although not the focus of our discussion in this paper, we note that for the same temperature change, as the thickness of the polysilicon layer is decreased from 3.5 to 1.5 μm, the magnitude of the curvature developed in the gold/polysilicon microstructure is increased while the magnitude of the stress in the gold layer is decreased. We attempted to use the same values of n and A to predict the curvature evolution during the isothermal hold of the uncoated microstructures. The predictions do not agree well with the measurements as they significantly underestimate the curvature change. The source of the disagreement is not completely clear, but it is likely due to the inability of the simple power

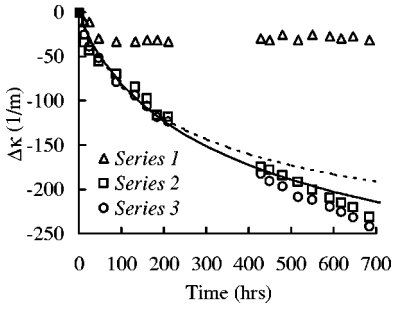

FIG. 10. Measured and predicted curvature change during the isothermal hold at 120 °C of 280 μm×50 μm gold (0.5 μm thick)/polysilicon (1.5 μm thick) beam microstructures. Open symbols represent the measurements and curves are calculations without (solid line) and with (dashed line) the coating.

law formulation to completely capture the actual deformation mechanisms. Recent studies on similar gold/polysilicon beams[30] suggest that in addition to the creep/stress-relaxation the deformation mechanisms may include recovery, and may change as a function of stress moving from a power law regime. The recovery mechanism results in tensile straining of the gold film, and it probably is necessary to include it in the constitutive model of the gold to obtain quantitative agreement for the deformation as a function of stress state (polysilicon thickness). The results, however, do resonate with similar studies of thin films on thick substrates in microelectronics contexts. For example, in their simulations of stress relaxation of metal films on thick substrates, Keller *et al.*[4] found that to obtain good agreement between predictions and measurements they could use a constant power-law exponent n, but they had to use a thickness-dependent activation energy and temperature-dependent dislocation density. Furthermore, unlike their situation with a thick substrate relative to the film, in our samples there are substantial stress variations through the thickness of the layers since they are of comparable thickness. The stress gradient in the 0.5-μm-thick gold/1.5-μm-thick polysilicon film is higher than that in the 0.5-μm-thick gold/3.5-μm-thick polysilicon film, although the magnitude of the stress is less. Because of the change in stress gradient with polysilicon thickness (Fig. 13), it is possible that the gold material regions being ''sampled'' by high stresses in the two different beams have different microstructures since microstructure changes throughout film thickness. For example, the smaller stress gradient in the 0.5-μm-thick gold/3.5-μm-thick polysilicon beams would cause relatively high stress across the entire gold film. By way of contrast, the steep gradient in the 0.5-μm-thick gold/1.5-μm-thick polysilicon beams would concentrate stresses at the interface, thus biasing the sample of different microstructures. In the calculations, if we keep $n=5$, but increase A to $5.2\times10^{-15}\,\mathrm{h}^{-1}\,\mathrm{MPa}^{-5}$, we obtain good agreement between the predictions and measurements for the uncoated microstructures. The same power-law parameters were used to model the coated microstructures and the predictions significantly overestimate the stress relaxation in these coated microstructures. Figure 10 shows the curvature change during the isothermal hold at 120 °C of 280 μm×50 μm gold (0.5 μm thick)/polysilicon (1.5 μm thick) beam microstruc-

Downloaded 12 Jul 2004 to 128.138.222.15. Redistribution subject to AIP license or copyright, see http://jap.aip.org/jap/copyright.jsp

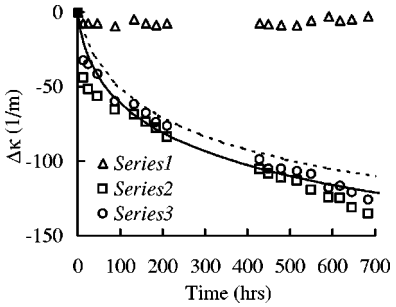

FIG. 11. Measured and predicted curvature change during the isothermal hold at 120 °C of 200 μm×200 μm gold (0.5 μm thick)/polysilicon (1.5 μm thick) plate microstructure. Open symbols represent the measurements and curves are calculations without (solid line) and with (dashed line) the coating.

tures. Similar to the gold with 3.5-μm-thick polysilicon beam microstructures shown in Fig. 8, the presence of the coating layer has a significant effect on the relaxation of curvature. For the uncoated beams, after 700 h, about 45% of the initial curvature is relaxed. However, for the coated beams, only about 4% of the initial curvature is relaxed.

In Figs. 11 and 12 we compare predictions and calculations of the relaxation behavior of the plates with 1.5 μm polysilicon films, using $n=5$ and $A=5.2\times10^{-15}\,\mathrm{h}^{-1}\,\mathrm{MPa}^{-5}$, since it adequately describes the behavior of the uncoated beams in Fig. 10. Figure 11 shows the measured and predicted results for the $L=200\,\mu$m plate. Both the measurements and predictions show that the deformation of this microstructure is symmetric, i.e., there is no bifurcation. Curvatures in both the x and y directions are measured and they are roughly the same. In Fig. 11 only the curvature in the x direction is shown. The plate microstructures show similar behavior to that of the beams in Fig. 10.

Figure 12 shows corresponding measurements and predictions for the $L=300\,\mu$m plates. The situation is quite different qualitatively, though. At the initial point of the stress relaxation process, the microstructure is deformed into an ellipsoidal shape, i.e., $\kappa_x\neq\kappa_y$. This is because during the cooling process the equilibrium shape of the gold/polysilicon plate has changed from one exhibiting essentially spherical curvature to a buckled mode where the curvature is essentially ellipsoidal (for a detailed discussion regarding the deformation and structural stability of layered plate microstructures subjected to thermal loading, please see Dunn *et al.*[18]). During the isothermal hold for the uncoated plates, the curvature κ_x decreases while κ_y increases, and the rate of decrease of κ_x is greater than that of the increase of κ_y. Both measurements and predictions show this, although there are quantitative differences. Over time both κ_x and κ_y evolve significantly from their values at $t=0$, indicating that the plate is trying to unbuckle from an ellipsoidal shape to a circular shape (see also Zhang and Dunn[10]). For the coated plate, the microstructure initially deforms into an ellipsoidal shape also, though, the initial curvature of the coated plate is smaller than that of the uncoated plates. During the isothermal hold, there is no significant increase or decrease of κ_x, while κ_y decreases slightly during the whole time period for the coated plate. The maximum curvature change $\Delta\kappa_x$ is 5.6 1/m (about 1.85% of the initial curvature). After 700 h, about 15% of the initial κ_y is relaxed.

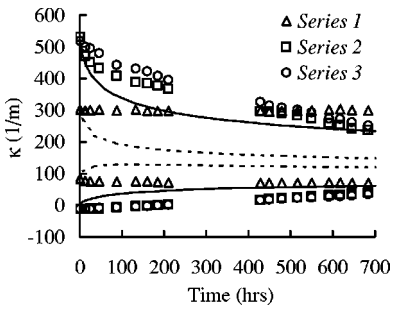

FIG. 12. Measured and predicted curvature during the isothermal hold at 120 °C of 300 μm×300 μm gold (0.5 μm thick)/polysilicon (1.5 μm thick) plate microstructure. Open symbols represent the measurements and curves are calculations without (solid line) and with (dashed line) the coating.

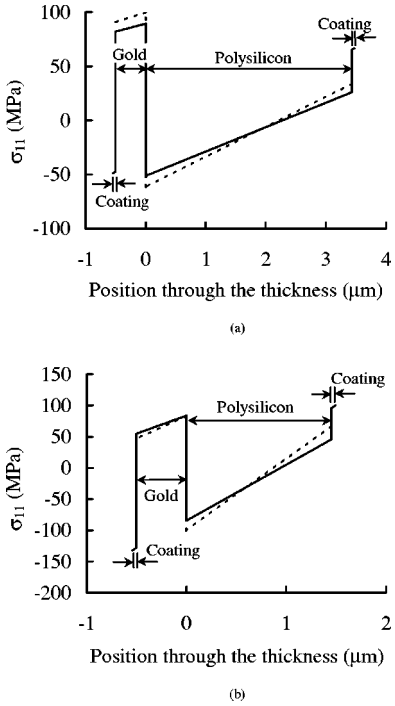

FIG. 13. Calculated stress distributions at the center of the cantilever beam microstructures through the thickness for (a) gold (0.5 μm thick)/polysilicon (3.5 μm thick) and (b) gold (0.5 μm thick)/polysilicon (1.5 μm thick) beam microstructures at $t=0$ during the isothermal hold. Solid lines and dashed lines represent calculations with and without the coating, respectively.

While we focus on the deformation of the microstructures, in Fig. 13 we show the corresponding stress distributions through the thickness for both coated and uncoated gold/polysilicon beam microstructures at the starting point $(t=0)$ of the isothermal hold. Compared with the stress in the uncoated beams, the magnitude of the stress in gold and polysilicon layers does not change significantly for the coated beams, however the stress gradient in both layers is decreased. The decrease of the stress gradient in the gold layer is more noticeable for the beams with thinner polysilicon. The stress in the Al_2O_3 coating layers is in compression in the layer adjacent to the gold and in tension in the layer adjacent to the polysilicon.

Downloaded 12 Jul 2004 to 128.138.222.15. Redistribution subject to AIP license or copyright, see http://jap.aip.org/jap/copyright.jsp

VI. CONCLUSIONS

We studied the suppression of inelastic deformation in multilayer film (gold/polysilicon) microstructures by alumina nanocoatings deposited by atomic layer deposition. With nanocoatings of 40 nm, the thermoelastic behavior ($d\kappa/dT$) is slightly altered. The measured curvature was used to estimate Young's modulus of the amorphous ALD alumina and the result is in reasonable agreement with published results in the literature. During the isothermal holds the curvature changes significantly with time, but the nanocoating largely suppresses the curvature change. We modeled the curvature evolution using the simple assumption that the inelastic deformation mechanism can be described by a power law, $\dot{\epsilon} = A\sigma^n$, and that the polysilicon and alumina deform elastically. The predictions describe the observed behavior reasonably well for the uncoated microstructures, however, for coated microstructures, predictions far underestimate the suppression of curvature evolution. We are not sure about the deformation mechanisms causing this to happen. Probably the coating layer will prevent surface atomic diffusion and constrain dislocation motion[9] requiring the use of a different creep model for coated and uncoated beams.

ACKNOWLEDGMENTS

This effort is sponsored by the Sandia National Laboratories/National Science Foundation Lifecycle Engineering Program and the Air Force Office of Scientific Research (F49620-02-1-0037). We are grateful to Dudley Finch for obtaining the SEM picture.

[1] D. C. Miller, W. Zhang, and V. M. Bright, Sens. Actuators, A **89**, 76 (2001).
[2] D. J. Vickers-Kirby, R. L. Kubena, F. P. Stratton, R. J. Joyce, D. T. Chang, and J. Kim, Mater. Res. Soc. Symp. Proc. **67**, EE2.5.1 (2001).
[3] D. Weiss, H. Gao, and E. Arzt, Acta Mater. **49**, 2395 (2001).
[4] R. M. Keller, S. P. Baker, and E. Arzt, Acta Mater. **47**, 415 (1999).
[5] Y. L. Shen and S. Suresh, Acta Metall. Mater. **43**, 3915 (1995).
[6] M. D. Thouless, J. Cupta, and J. M. E. Harper, J. Mater. Res. **8**, 1845 (1993).
[7] M. D. Thouless, Annu. Rev. Mater. Sci. **25**, 69 (1995).
[8] M. D. Thouless, K. P. Rodbell, and C. Cabral, J. Vac. Sci. Technol. A **14**, 2454 (1996).
[9] Y. L. Shen and U. Ramamurty, J. Appl. Phys. **93**, 1806 (2003).
[10] Y. Zhang and M. L. Dunn, J. Mech. Phys. Solids (to be published).
[11] D. A. Koester, R. Mahadevan, B. Hardy, and K. W. Markus, *MUMPs™ Design Rules*, Cronos Integrated Microsystems, A JDS Uniphase Company, 2001, http://www.memsrus.com/cronos/svcsrules.html
[12] S. M. George, A. W. Ott, and J. W. Klaus, J. Phys. Chem. **100**, 13121 (1996).
[13] M. Ritala and M. Leskela, in *Handbook of Thin Film Materials*, edited by H. S. Nalwa (Academic, San Diego, 2001).
[14] A. W. Ott, J. W. Klaus, J. W. Johnson, and S. M. George, Thin Solid Films **292**, 135 (1997).
[15] J. W. Elam, M. D. Groner, and S. M. George, Rev. Sci. Instrum. **73**, 2981 (2002).
[16] N. D. Hoivik, J. W. Elam, R. J. Linderman, V. M. Bright, S. M. George, and Y. C. Lee, Sens. Actuators, A **103**, 100 (2003).
[17] J. W. Elam and S. M. George, Chem. Mater. **15**, 1020 (2003).
[18] M. L. Dunn, Y. Zhang, and V. Bright, J. Microelectromech. Syst. **11**, 372 (2002).
[19] Y. Zhang and M. L. Dunn, J. Microelectromech. Syst. **12**, 788 (2003).
[20] W. D. Nix, Metall. Trans. A **20A**, 2217 (1989).
[21] J. Koike, S. Utsunomiya, Y. Shimoyama, K. Maruyama, and H. Oikawa, J. Mater. Res. **13**, 3256 (1998).
[22] S. P. Baker, A. Kretschmann, and E. Arzt, Acta Mater. **49**, 2145 (2001).
[23] M. Legros, K. J. Hemker, A. Gouldstone, S. Suresh, R.-M. Keller-Flaig, and E. Artz, Acta Mater. **50**, 3435 (2002).
[24] K. Gall, M. L. Dunn, Y. Zhang, and B. Corff, Mech. Mater. **36**, 45 (2004).
[25] W. N. Sharpe, in the *MEMS Handbook*, edited by M. Gad-el-Hak (CRC Press, Boca Raton, FL, 2002).
[26] J. A. King, *Materials Handbook for Hybrid Microelectronics* (Teledyne Microelectronics, Los Angeles, 1988).
[27] F. DelRio *et al.* (private communication).
[28] J. Proost and F. Spaepen, J. Appl. Phys. **91**, 204 (2002).
[29] W. D. Callister, *Materials Science and Engineering An Introduction* (Wiley, New York, 1997).
[30] K. Gall, N. West, K. Spark, M. L. Dunn, and D. Finch, Acta Mater. **52**, 2133 (2004).

Downloaded 12 Jul 2004 to 128.138.222.15. Redistribution subject to AIP license or copyright, see http://jap.aip.org/jap/copyright.jsp